Active and passive Brownian motion of charged particles in two-dimensional plasma models

Jörn Dunkel,[1] Werner Ebeling,[1] and Sergey A. Trigger[2,*]
[1]*Institut für Physik, Humboldt-Universität zu Berlin, Newtonstraße 15, D-12489 Berlin, Germany*
[2]*Joint Institute for High Temperatures, Russian Academy of Science, Izhorskaya 13/19, 127412 Moscow, Russia*
(Received 19 December 2003; revised manuscript received 4 May 2004; published 13 October 2004)

The dynamics of charged Coulomb grains in a plasma is numerically and analytically investigated. Analogous to recent experiments, it is assumed that the grains are trapped in an external parabolic field. Our simulations are based on a Langevin model, where the grain-plasma interaction is realized by a velocity-dependent friction coefficient and a velocity-independent diffusion coefficient. In addition to the ordinary case of positive (passive) friction between grains and plasma, we also discuss the effects of negative (active) friction. The latter case seems particularly interesting, since recent analytical calculations have shown that friction coefficients with negative parts may appear in some models of ion absorption by grains as well as in models of ion-grain scattering. Such negative friction may cause active Brownian motions of the grains. As our computer simulations show, the influence of negative friction leads to the formation of various stationary modes (rotations, oscillations), which, to some extent, can also be estimated analytically.

DOI: 10.1103/PhysRevE.70.046406 PACS number(s): 52.27.Lw, 05.40.Jc, 52.20.Hv

I. INTRODUCTION

During the last two decades the physics of charged grains in plasmas has attracted ever-growing theoretical [1–5] and experimental interest [6–9]. Among the first who theoretically investigated the dynamics of finite, two-dimensional (2D) Coulomb clusters with parabolic confinement were Lozovik and co-workers [2,3], Bolton and Rössler [4], and Bedanov and Peeters [5]. Using Monte Carlo simulation techniques, these authors were able to develop a classification scheme ("Mendeleev table") of the elementary excitations in systems with $N=2,\ldots,52$ grains. Later, Schweigert and Peeters investigated the spectral properties of classical (nonquantum) 2D Coulomb clusters on the basis of a modified Newton method [10]. In this context, one should also mention recent dynamical simulations performed by Bonitz *et al.* [11].

Experimental interest in 2D Coulomb systems was stimulated by the discovery of dusty plasmas, containing relatively large highly charged grains [6,12–15]. Since then, the dynamics of Coulomb clusters has been studied in various experiments [7–9,16–18]. For example, relatively long living oscillatory and rotational modes have been observed [18,19] and also theoretically investigated [1,20–27]. Another remarkable observation is that in some experiments the grains are characterized by very large kinetic energy values, corresponding to a temperature three to ten times higher than that of the electrons in the plasma [8,9,14,16,28]. Reviews discussing some of these phenomena can be found in [29–33].

In the present paper, we investigate numerically and analytically the dynamics of confined Coulomb grains on the basis of Langevin equations with nonlinearly velocity-dependent friction coefficients. This approach does differ essentially from the Monte Carlo techniques [2–5] and the Newton method [10], as used by other authors in preceding investigations. In particular, we will also take into account the possibility of friction functions possessing negative parts. Since Lord Rayleigh's work on sustained sound oscillations [34], negative friction has become a useful concept for modeling complex energy input processes in a simple manner. With regard to dusty plasmas, negative friction has until now been considered in specific physical models only, which have to be further developed in order to be applicable to experimentally realized dusty plasmas [16,17,19].

In a number of recent theoretical papers the stochastic dynamics of charged grains in plasmas has been discussed in the framework of Brownian motions [27,35–41]. In particular, for a relatively simple solvable grain-plasma interaction model [41], it was shown that there appear some parallels to the theory of active Brownian particles [42–45]. If a grain in a plasma is regarded as a Brownian particle, then the friction function $\gamma(\boldsymbol{v})$ provides an averaged macroscopic description of the forces due to the grain-plasma interactions ($\boldsymbol{v}$ denotes the velocity vector of a grain). The explicit shape of the function $\gamma(\boldsymbol{v})$ is exclusively determined by the underlying microscopic model, considered to describe the relevant microscopic interaction processes between the grains and surrounding plasma particles (electron, ion and atom scattering, absorption and emission of plasma particles by grains, etc.). Thus, depending on which microscopic processes are taken into account, the friction function $\gamma(\boldsymbol{v})$ may differ considerably.

Intuitively, one would expect that the interaction with a plasma always leads to a damping of the grain motion, corresponding to generally positive friction $\gamma(\boldsymbol{v})>0$. Very recently, however, Trigger and Zagorodny [41] showed that there also exist acceleration effects which give negative contributions to the friction function. More exactly, these authors considered a relatively simple, analytically solvable model for a fully ionized plasma with dominating ion-grain charging collisions. This model takes into account the momentum transfer between ions and and grains, but neglects mass transfer processes. For this specific model it was found that,

*Electronic address: strig@gmx.net

under certain conditions, there can exist a nonvanishing absolute velocity value $v_0 > 0$, such that the effective friction coefficient $\gamma(\boldsymbol{v})$ is negative for $|\boldsymbol{v}| < v_0$ and positive for $|\boldsymbol{v}| > v_0$. Additionally, for this model the velocity space diffusion coefficient $D(\boldsymbol{v})$ was determined by means of a self-consistent calculation [in contrast to $\gamma(\boldsymbol{v})$ the function $D(\boldsymbol{v})$ is always positive].

Negative friction for small grain velocities means that slow grains (with $0 < |\boldsymbol{v}| < v_0$) are accelerated in the direction of their motion due to some specific, unbalanced momentum transfer mechanism. An example for such a mechanism is the charging collisions considered in [41]. Qualitatively, this process can be summarized as follows. A negatively charged grain attracts positively charged plasma ions in its neighborhood, which are finally absorbed at its surface. If the grain is at rest in the plasma, then there is effectively no momentum transfer during the absorption process. In contrast, for slowly moving grains, the positive net acceleration stemming from tailside absorptions may be larger than the negative acceleration due to frontside absorptions, thus leading to an effective (counterintuitive) acceleration of the grains in the direction of their motion. It is necessary to emphasize (as was already done earlier [36,37,41]) that this effect was found for a specific model, which is based on the standard assumption that mass transfer is negligible. This model is valid for time scales of the order of the charging processes and provides the correct values of the average grain charge and charge distribution. However, it can be insufficient for larger time scales, for which the increase of the grain mass may become essential. Therefore, until now it is still an open question whether the simple model discussed [41] can be applied in order to correctly calculate the friction forces acting on long time scales in real dusty plasmas. For the correct calculation of these forces, it may be necessary to take into account the kinetics of ion recombination with electrons on the dust surface and the subsequent removal of the created atoms to the ambient plasmas. An approach to this problem has already been discussed in [37,38], but a complete theory of such processes has not yet been considered.

On the other hand, not only ion-grain charging collisions may yield friction functions with negative parts. Under certain conditions (e.g., in the presence of an ion flow in the plasma), scattering of ions by grains may lead to negative friction as well [46]. In particular, it seems that this effect can be responsible for some observations in the experiments by Dahiya *et al.* [19]. Hence, in principle, one cannot exclude that active motions of grains can occur for some specific dusty plasma parameters and conditions, since there exist several different mechanisms that can give negative contributions to the friction coefficient $\gamma(\boldsymbol{v})$.

In the meantime, it seems reasonable to identify the peculiarities that arise for qualitatively different types of friction coefficients. Therefore, it is the primary aim of this paper to study the effects of positive and negative friction on the dynamics of 2D Coulomb clusters from a general point of view. To this end, we have performed computer simulations of the cluster dynamics for two qualitatively different phenomenological friction models, corresponding to passive and active friction, respectively.

As mentioned before, in contrast to previous numerical investigations [4,5,10] of finite 2D Coulomb clusters, the results presented below were obtained by direct numerical integration of the Langevin equations, governing the stochastic dynamics of the grains in the plasma. Compared with Monte Carlo techniques [4,5] and the Newton method [10], this approach has the advantage that one obtains detailed time-dependent trajectories of the 2D Coulomb system. Moreover, the Langevin method is readily applicable to a wide class of models with nonlinearly velocity-dependent friction and diffusion coefficients.

Formally, the paper is structured as follows. In Sec. II we briefly review general aspects concerning the Brownian motion of isolated Coulomb grains in plasmas. The Langevin equations for interacting grains are discussed in Sec. III. As shown in Sec. IV, the Langevin approach can successfully reproduce experimental data for the common case of positive (passive) friction. Section V focuses on the effects of negative (active) friction. Section VI contains a summary of the main results.

II. BROWNIAN MOTION OF FREE GRAINS IN PLASMAS

In this section we briefly discuss the Brownian motion of an isolated dust grain (i.e., grain-grain interactions are neglected in this part).

A. Langevin and Fokker-Planck equations of a free grain

Consider a negatively charged grain with position vector $\boldsymbol{r}(t)$, velocity vector $\boldsymbol{v}(t)$, and unit mass $m_g = 1$. The two-dimensional Brownian motion of such a grain in a surrounding plasma can be described by the Langevin equation

$$\frac{d}{dt}\boldsymbol{r} = \boldsymbol{v}, \tag{1a}$$

$$\frac{d}{dt}\boldsymbol{v} = -\gamma(v)\boldsymbol{v} + \sqrt{2D(v)}\boldsymbol{\xi}(t), \tag{1b}$$

where the stochastic force term is characterized by the time averages

$$\langle \boldsymbol{\xi}(t) \rangle = \mathbf{0}, \quad \langle \xi_\nu(t)\xi_\mu(s) \rangle = \delta_{\nu\mu}\,\delta(t-s) \tag{2}$$

with $\mu, \nu = 1, 2$ denoting the two spatial components of the random vector $\boldsymbol{\xi}$. In the Langevin approach, the friction coefficient γ and the velocity diffusion coefficient D give an averaged *macroscopic* description of the grain-plasma interactions.

Throughout this paper, we shall confine ourselves to the case where the plasma is isotropic in the horizontal x-y plane in which the charged grains are moving. Note that this does not exclude the possibility of a vertical anisotropy in the plasma (i.e., an anisotropy with respect to the third spatial direction z). For such isotropic 2D plasmas the coefficients γ and D are nonlinear functions of the absolute velocity $v = |\boldsymbol{v}|$ of the grain. By considering the energy balance equation associated with Eq. (1), one can easily see that the function $\gamma(v)$ models the energy transfer from the plasma to the grain. For example, under typical experimental conditions there may also exist vertical currents, crossing the x-y plane in the

z direction, which of course also transfer energy to the grains. Therefore, one should consider $\gamma(v)$ as a phenomenological model for the energy transfer from three different directions to the grains. Due to the complex character of the grain-plasma interactions, a complete microscopic theory does not yet exist. However, there exist special tractable models for which the (in general nonlinear) functions $\gamma(v)$ and $D(v)$ can be calculated.

For example, in [35–38,41] explicit functional expressions for $\gamma(v)$ and $D(v)$ were derived on the basis of *microscopic* models of the interaction between the grain and the plasma constituents. The exact shape of the corresponding coefficients essentially depends on the underlying microscopic model and, in particular, on the microscopic processes taken into account. A more detailed discussion concerning the structure of $\gamma(v)$ will be given below in Sec. II B. First, let us briefly discuss the stationary velocity distribution that follows from the Langevin dynamics (1).

In order to find the stationary velocity distribution for a grain governed by Eq. (1), one can use the corresponding Fokker-Planck equation (FPE) for the probability density function $f(\boldsymbol{r},\boldsymbol{v},t)$. The FPE reads

$$\frac{\partial f}{\partial t}+\boldsymbol{v}\frac{\partial f}{\partial \boldsymbol{r}}=\frac{\partial}{\partial \boldsymbol{v}}\left[\gamma(v)\boldsymbol{v}f+\frac{\partial D(v)f}{\partial \boldsymbol{v}}\right]. \tag{3}$$

The stationary solution of this equation is well known (see, e.g., [41]):

$$f(\boldsymbol{v})=\frac{C}{D(v)}\exp\left(-\frac{1}{2}\int\frac{\gamma(v)}{D(v)}dv^2\right). \tag{4}$$

For constant friction and diffusion coefficients, i.e., for $\gamma(v)\equiv\gamma_0$ and $D(v)\equiv D_0$, this solution corresponds to a Maxwellian (Gaussian) velocity distribution. In the case of more realistic plasma models, however, the velocity distribution (4) is non-Maxwellian.

Qualitatively, the two simplest cases one can distinguish are monostable and bistable distributions $f(\boldsymbol{v})$. Monostable distributions, such as e.g., the Maxwell distribution, are associated with purely positive friction coefficients $\gamma(v)>0$. If the friction function $\gamma(v)$ is purely positive (and slowly varying), then one may use the simple approximation by a constant $\gamma(v)\simeq\gamma_0$. A completely different distribution results if the friction function becomes negative at small velocities. More exactly, it has been shown that multimodal distributions appear if $\gamma(v)$ may assume negative values for some velocity domain [41,47,48].

The transition from purely positive friction coefficients to friction functions exhibiting a negative part can be viewed as a bifurcation. A common procedure in bifurcation theory (as well as in the theory of phase transitions) is to use a low order Taylor expansion near the bifurcation point. Since $\gamma(v)$ should be an even function, this leads in lowest order to Rayleigh's phenomenological model of active friction [34]

$$\gamma_R(v)=-\beta+\alpha v^2=\alpha(v^2-v_0^2),\quad \alpha>0, \tag{5}$$

where $v_0^2=\beta/\alpha$. Near the bifurcation point, the constant β and correspondingly also the characteristic velocity v_0 are relatively small. Additionally, in this situation one may also simplify the diffusion function by assuming that $D(v)\simeq D_0>0$. Obviously, in the Rayleigh model (5) the friction coefficient is negative if $v^2<v_0^2$ and positive otherwise. According to Eq. (4), the related stationary velocity distribution function is then given by

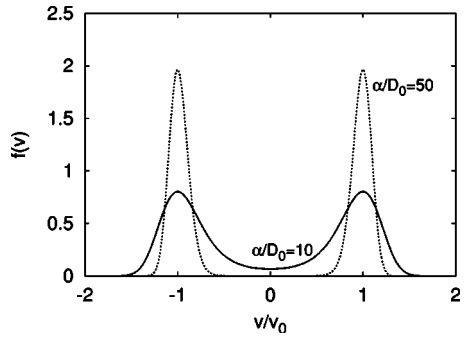

FIG. 1. Non-Maxwellian stationary distribution function for the Rayleigh friction model $\gamma_R(v)=\alpha(v^2-v_0^2)$ from Eq. (5). In the limit $\alpha/D_0\to 0$ the density converges to the δ-function (7).

$$f(\boldsymbol{v})=\mathcal{N}\exp\left[-\frac{\alpha}{4D_0}(v^2-v_0^2)^2\right], \tag{6}$$

where $\mathcal{N}$ is a normalization constant. As one can see in Fig. 1, the probability density $f(\boldsymbol{v})$ exhibits two peaks near $\pm v_0$ and decays strongly at high absolute velocities. In the weak noise limit, $D_0/\alpha\to 0$, the distribution becomes very narrow around $\pm v_0$, approaching the δ distribution

$$f_0(\boldsymbol{v})=\tilde{\mathcal{N}}\delta(\boldsymbol{v}^2-v_0^2). \tag{7}$$

That is, in this limit the dispersion of the kinetic energy of the grains is completely neglected. From the physical point of view, the Brownian grains then move with constant kinetic energy $E=m_g v_0^2/2$, while randomly changing their directions of motion from time to time.

To summarize, if the negative friction effects are relatively weak, then it is often sufficient to approximate a more complicated friction function $\gamma(v)$ by Rayleigh's simple model (5), which is effectively characterized by only two parameters α and v_0.

B. Structure of the friction coefficient in more realistic plasma models

Starting from detailed microscopic models of the grain-plasma interaction, it is in principle possible to derive explicit functional expressions for $\gamma(v)$ and $D(v)$. Then, of course, the results do essentially depend on the properties of the underlying microscopic model. For example, the qualitative behavior of $\gamma(v)$ and $D(v)$ strongly differs, depending on whether surface recombination effects between plasma ions and grain surface electrons are neglected or not, as discussed above.

Generally, for a plasma consisting of ions and atoms the friction coefficient can be written in the additive form

TABLE I. Typical grain, plasma, and trap parameters as given in [7] for a helium plasma containing charged spherical plastic particles. The last column gives the corresponding parameter values in the characteristic units (c.u.) as used in our computer simulations. At temperature $T=300$ K and $Z_i=1$ these parameters result in $\Gamma \approx 140$ (ion-grain interaction parameter).

Quantity	Symbol	Value (SI units)	Value (c.u.)
Grain radius	a	4.74 μm	0.0053
Grain mass	m_g	6.73×10^{-13} kg	1
Grain charge	Q	$-12100e$	-12100
Debye length	λ_D	900 μm	1
Viscous friction coefficient	γ_0	5.5 s^{-1}	0.67
Pressure	P	1.6 Pa	
Trap angular frequency	ω_0	$2\pi\times1.3$ s^{-1}	1
Permittivity of free space	ε_0	8.85×10^{-12} F m^{-1}	
Boltzmann constant	k	1.38×10^{-23} J K^{-1}	

$$\gamma(v) = \gamma_n(v) + \gamma_i(v). \tag{8}$$

Here, $\gamma_n(v)$ is related to grain–neutral-atom collisions, and $\gamma_i(v)$ represents the influence of ion absorptions and scattering. In the next two sections we briefly discuss some general properties of $\gamma_n(v)$ and $\gamma_i(v)$.

1. Atomic friction

Under the usual experimental conditions the plasmas are often weakly ionized, i.e., in addition to ions and electrons the plasma also contains a non-negligible amount of neutrals species (atoms). Therefore, a reasonable theory must also take into account the interactions between the grains and the neutrals atoms. Analytical estimates of this effect on the basis of the kinetic theory are well known [49]. In principle, grain–neutral-atom interactions always give rise to a positive contribution $\gamma_n(v)>0$ to the full friction coefficient $\gamma(v)$; that is, such interactions always lead to *passive* friction.

Throughout this paper, we shall assume that it is sufficient to use an Epstein-type [49] approximation in order to account for grain–neutral-atom collisions; i.e., we confine ourselves to the case

$$\gamma_n(v) \equiv \gamma_0, \tag{9}$$

where γ_0 is a positive constant. This simplifying assumption is also justified by analytical results based on the transition probability function for the short-range atom-grain interaction [50]. For the case of a mirror reflection of the point atoms from the spherical grain the expression for the atomic friction can be represented as [50]

$$\gamma_0 = 8A\frac{n_a}{n_i}\left(\frac{T_a m_a}{T_i m_i}\right)^{1/2}, \tag{10}$$

where

$$A = \frac{1}{3}\sqrt{2\pi}\left(\frac{m_i}{m_g}\right)a^2 n_i v_{\mathrm{Ti}}. \tag{11}$$

The quantities appearing in Eqs. (10) and (11) are the grain mass m_g, the grain radius a, the mass m_a of an atom, the densities $n_{i/a}$ of ions and atoms in the plasma, the ion mass m_i, and the thermal ion temperature

$$v_{\mathrm{Ti}}^2 \equiv \frac{kT_i}{m_i}. \tag{12}$$

In typical experiments [7,18] the passive friction coefficient γ_0 is of the order $1-10$ s^{-1} (see Table I).

2. Grain-ion interaction

Rather generally, the ionic contribution $\gamma_i(v)$ to the full friction coefficient (8) can be written in the form

$$\gamma_i(v;\Gamma) = \gamma_i^a(v;\Gamma) + \gamma_i^s(v;\Gamma) + \gamma_i^r(v;\Gamma). \tag{13}$$

Here, γ_i^a reflects the absorption of ions at the surface of the grain, while γ_i^s represents friction resulting from scattering processes between the negatively charged grain and positively charged plasma ions. The last term γ_i^r is connected with surface recombination processes. As discussed in [36,50], a satisfactory theory of grain-plasma interactions must also account for the recombination of absorbed ions and electrons in the grain as well as for the subsequent removal of the emerging atoms from the grain surface to the surrounding plasma. Such a theory, however, is still absent.

As indicated by the notation, the explicit shape of γ_i is essentially determined by the characteristic ion-grain interaction parameter

$$\Gamma \equiv \frac{Z_g Z_i e^2}{4\pi\varepsilon_0\, a\, kT_i}, \tag{14}$$

where Z_g and Z_i are the charge numbers of the grains and the plasma ions, respectively, while a denotes the grain radius and T_i is the ion temperature in the plasma.

An analytical expression for the absorption coefficient γ_i^a has been calculated earlier [41] for the specific model discussed in Sec. I. An interesting aspect of this model is that γ_i^a assumes negative values for small absolute velocity, if the degree of ionization in the plasma is sufficiently high. Another cause of negative friction in quite realistic models can be the existence of ion flows. For example, when an ion

stream is flowing in a dusty plasma the friction coefficient $\gamma(v)$ behaves as $-1/v$ for small absolute velocity values [46,50]. This result means that under such special (anisotropic) conditions negative friction effectively always exists due to ion flow scattering by grains. In this case the ion drag force, recently calculated also for large angles of ion scattering [39,51], leads to a negative term in the effective friction coefficient. For example, as shown in [51], for moderate parameter values

$$\frac{Z_g e^2}{4\pi\varepsilon_0\,\lambda_D\,m_i v_i^2} < 5, \tag{15}$$

the ion-grain scattering friction coefficient γ_i^s takes the form

$$\gamma_i^s(\Gamma) = 2A\Gamma^2 \ln\,\Lambda, \tag{16}$$

where $\ln\,\Lambda$ is the Coulomb logarithm generalized to dusty plasmas [39,40].

Since negative friction manifests itself in several dusty plasma models, it seems reasonable to consider the specific properties of the grain dynamics in the presence of grain-grain interactions, not only for the case of positive friction, but also for negative friction.

III. DYNAMICS OF CONFINED CLUSTERS OF CHARGED GRAINS

A. Screened interactions and equations of motion

In the previous sections, the interaction between quasifree grains and a surrounding plasma has been discussed. In the remainder, we additionally consider grain-grain interactions, mediated by a screened Coulomb pair interaction potential

$$\Phi_{ij}^{\mathrm{C}}(r) = \frac{Q_i\,Q_j}{4\pi\varepsilon_0}\frac{1}{r_{ij}}\exp\left(-\frac{r_{ij}}{\lambda_D}\right), \tag{17}$$

where

$$r_{ij} = |\boldsymbol{r}_i - \boldsymbol{r}_j| \tag{18}$$

denotes the distance between two grains located at $\boldsymbol{r}_i = (x_i, y_i)$ and $\boldsymbol{r}_j = (x_j, y_j)$, respectively. For simplicity, we shall confine ourselves to the case where all grains are identical, i.e.,

$$Q_i = Q = -Z_g e \tag{19}$$

for all $i = 1, 2, \ldots, N$. We also note that deviations from the Debye potential, which may be caused by different attraction mechanisms (shadow effects, dipole interactions, etc.), are negligible for the parameter range considered in the present paper (see, e.g., [30,31] for an extensive discussion of the limitations of the Debye interaction model). Similarly, the influence of ion wake fields can be neglected, as long as the typical velocity of the grains is smaller than the thermal velocity of the ions.

If an ensemble of N Coulomb grains is confined by an external parabolic potential

$$\Phi^{\mathrm{ext}}(\boldsymbol{r}) = \frac{m_g\omega_0^2}{2}\boldsymbol{r}^2, \tag{20}$$

then the ground-state configuration corresponds to a regular two-dimensional structure, referred to as Coulomb crystal [4,10,52]. These structures can be classified, and for the case of pure Coulomb interactions, corresponding to $\lambda_D \to \infty$, a Mendeleev table for particle numbers $N = 2, \ldots, 52$ was presented in Ref. [5]. An analogous analysis for screened potentials of the type (17) is, e.g., given in [53].

In the present paper we are going to study the dynamics of two-dimensional Coulomb clusters in a harmonic trap by using a Langevin approach. In particular, we are interested in identifying the excitations that may arise due to the influence of negative friction. To this end, we numerically integrate the Langevin equations of motion

$$\dot{\boldsymbol{r}}_i = \boldsymbol{v}_i, \tag{21a}$$

$$\dot{\boldsymbol{v}}_i = (\boldsymbol{F}_i^{\mathrm{C}} + \boldsymbol{F}_i^{\mathrm{ext}})/m_g - \gamma(v_i)\boldsymbol{v}_i + \sqrt{2D_0}\,\boldsymbol{\xi}_i(t), \tag{21b}$$

where $\boldsymbol{x}_i$ describes the position of a grain at time t and $\boldsymbol{v}_j$ denotes its velocity. The external linear force $\boldsymbol{F}_i^{\mathrm{ext}}$ modeling the ion trap reads

$$\boldsymbol{F}_i^{\mathrm{ext}} = -\nabla_i\Phi^{\mathrm{ext}}(\boldsymbol{r}_i) = -m_g\omega_0^2\,\boldsymbol{r}_i, \tag{22}$$

and the screened Coulomb force is obtained from

$$\begin{aligned}\boldsymbol{F}_i^{\mathrm{C}} &= -\nabla_i\sum_{j=1,j\neq i}^{N}\frac{Q^2}{4\pi\varepsilon_0}\frac{1}{r_{ji}}\exp\left(-\frac{r_{ji}}{\lambda_D}\right)\\ &= \sum_{j=1,j\neq i}^{N}\frac{Q^2}{4\pi\varepsilon_0}\frac{\boldsymbol{r}_i-\boldsymbol{r}_j}{r_{ij}^3}\exp\left(-\frac{r_{ij}}{\lambda_D}\right)\left(1+\frac{r_{ij}}{\lambda_D}\right),\end{aligned} \tag{23}$$

where

$$\boldsymbol{\nabla}_i \equiv \left(\frac{\partial}{\partial x_i}, \frac{\partial}{\partial y_i}\right)$$

is the Nabla operator related to the coordinates of the ith particle. In the Langevin equation (21b) the interaction between the grains and the surrounding plasma is realized by the last two terms, containing the friction coefficient $\gamma(v_i)$ and the stochastic Langevin force $\sqrt{2D_0}\,\boldsymbol{\xi}_i(t)$ with properties (2). With regard to the friction coefficient, we shall concentrate below on the following two cases: (i) constant positive (passive) friction corresponding to $\gamma(v) \equiv \gamma_0$; (ii) velocity-dependent negative friction corresponding to the Rayleigh model $\gamma_R(v) = \alpha(v^2 - v_0^2)$.

Moreover, we make a second simplifying assumption by always considering a constant noise amplitude D_0 in Eq. (21b). In the limit of purely constant viscous friction, $\gamma(v) \equiv \gamma_0$, this assumption is unproblematic since then the Einstein relation

$$D_0 = \frac{\gamma_0 kT}{m_g} \tag{24}$$

holds. In general, however, one should expect that both the friction coefficient and also the noise amplitude are velocity dependent. Among others, this is evident from the explicitly

velocity-dependent results for friction and diffusion coefficients given in [41]. Thus, using a constant noise amplitude parameter D_0 in the case of active friction reflects the assumption that the $D(v)$ is slowly varying around D_0. Since the main objective of this paper is to discuss the qualitative effects of active friction in two-dimensional Coulomb clusters, the simplification $D(v) \approx D_0$ seems reasonable at this stage.

In this context it should also be mentioned that friction and diffusion coefficients of dusty plasmas are, in general, functions of the grain charge [36]. For example, Matsoukas and Russel [54] and Schram *et al.* [40] have analyzed in detail the charge dependence of the stationary grain distribution function. According to their results, fluctuations of the grain charge are negligible if

$$\frac{e^2 Z_g^2}{4\pi\varepsilon_0\, a\, kT_{\mathrm{eff}}^*} \gg 1 \tag{25}$$

holds, where a denotes the grain radius and

$$T_{\mathrm{eff}}^* = T_e \frac{1+Z_i}{2} \frac{\vartheta+\zeta}{1+\vartheta+\zeta}, \quad \zeta = \frac{e^2 Z_g}{4\pi\varepsilon_0\, a\, kT_e}, \quad \vartheta = \frac{T_i}{Z_i T_e}. \tag{26}$$

Equation (25) is satisfied for the parameter values used in our computer simulations, and also for typical experimental conditions [7,18]. Therefore, following the standard approach [1], we neglect charge fluctuation effects by considering grains with constant identical charge values.

B. Characteristic unit system

It is convenient to use a characteristic unit (c.u.) system defined by

$$m_g = 1, \quad \lambda_D = 1, \quad e = 1, \quad \omega_0 = 1, \tag{27}$$

and to introduce the dimensionless coupling constant

$$\kappa \equiv \frac{Z_g^2 e^2}{4\pi\varepsilon_0 m_g \omega_0^2 \lambda_D^3}. \tag{28}$$

The experimental parameter values from Table I yield $\kappa = 1.03$, whereas $\kappa = 4.61$ for those from Table II. By virtue of Eq. (27) and (28) one can rewrite the Langevin equations (21) in the simplified form

$$\dot{\boldsymbol{r}}_i = \boldsymbol{v}_i, \tag{29a}$$

$$\dot{\boldsymbol{v}}_i = -\boldsymbol{r}_i + \boldsymbol{F}_i^C - \gamma(v_i)\boldsymbol{v}_i + \sqrt{2D_0}\,\boldsymbol{\xi}_i(t), \tag{29b}$$

where

$$\boldsymbol{F}_i^{\mathrm{C}} = \kappa \sum_{j=1, j\neq i}^{N} \frac{\boldsymbol{r}_i - \boldsymbol{r}_j}{r_{ij}^3} \exp(-r_{ij})(1+r_{ij}). \tag{29c}$$

Thus, the remaining effectively free parameters of the model are the coupling constant κ, the noise amplitude D_0, and the parameters of the friction model, i.e., γ_0 in the case of positive friction or α and v_0 if the Rayleigh model (5) is considered. Also note that all numerical results presented below will exclusively refer to Eqs. (29).

TABLE II. Typical grain, plasma, and trap parameters as determined in [18] for melamine-formaldehyde microspheres surrounded by an argon plasma. The last column gives the corresponding parameter values in the characteristic units (c.u.) as used in our computer simulations. At temperature $T = 300$ K and $Z_i = 1$ these parameters result in $\Gamma \approx 210$.

Quantity	Symbol	value (SI units)	Value (c.u.)
Grain radius	a	4.74 μm	0.0064
Grain mass	m_g	6.73×10^{-13} kg	1
Grain charge	Q	$-18000e$	-18000
Debye length	λ_D	740 μm	1
Viscous friction coefficient	γ_0	No data given	
Pressure	P	1.6 Pa	
Trap angular frequency	ω_0	7.7 s^{-1}	1

IV. POSITIVE (PASSIVE) FRICTION

In this section we concentrate on the limiting case of purely passive friction $\gamma(v) \equiv \gamma_0$. This case corresponds to experimental conditions as realized by Klindworth *et al.* [7] and Melzer *et al.* [18] (see Tables I and II). In the mentioned experiments the degree of ionization is rather low, $n_i \ll n_a$, and, therefore, ordinary positive friction due to grain-atom interactions is predominant.

In the context of the present paper, it is useful to consider $\gamma(v) \equiv \gamma_0$ first, because this case allows a straightforward comparison between our numerical simulations and the experimental results reported by Melzer *et al.* [18]. In this way one can check that the numerical integration of the Langevin equations (29) yields not only the correct ground-state configurations [5], but also the correct time-dependence of cluster oscillations. Moreover, with regard to the subsequent consideration of negative friction effects in Sec. V, it is useful to first discuss the case of passive friction.

It might be appropriate to emphasize that, compared with Monte Carlo methods [4,5], the Langevin approach has the advantage that it allows a time-resolved study of the grain dynamics. The Langevin method also makes it easy to numerically determine several stationary distributions for different nonlinearly velocity-dependent friction and diffusion coefficients, derived from microscopic models. These results can be compared with experimental data in order to evaluate the underlying microscopic theory.

Formally, this section is structured as follows. Section IV A contains analytical estimates for the simplest nontrivial case with $N=2$ grains. In Sec. IV B the stationary configurations of Coulomb crystals are determined via direct simulation of the dynamical equations (29) for the deterministic limit case $D_0 = 0$. The results presented in Sec. IV C show that the normal modes, as experimentally measured in [7], can also be numerically reproduced on the basis of the Langevin approach. Finally, in Sec. IV D numerically generated angular momentum distributions are discussed. As will become clear below, the analysis of angular momentum distributions might also provide a useful tool in order to determine whether or not negative friction is present in a system under consideration.

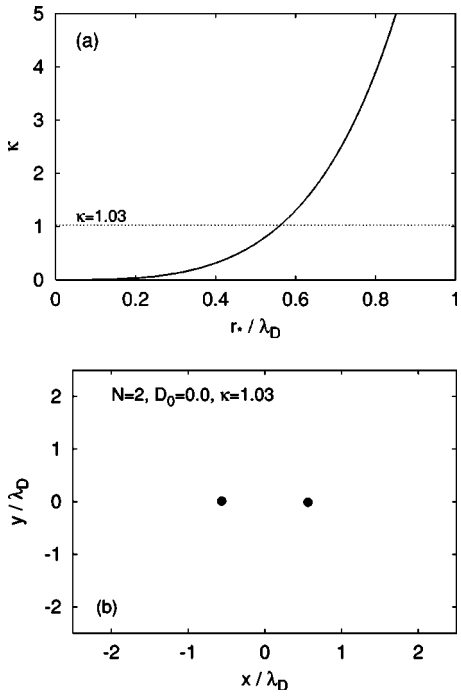

FIG. 2. (a) Solution $\kappa(r_*)$ of the transcendental equation (34). (b) Ground-state configuration for Coulomb crystals with $N=2$ grains (black dots) obtained from numerical simulations according to the procedure described in Sec. IV B. The stationary distance between the grains is given by $2r_*(\kappa)$, where $r_*(\kappa)$ is the inversion of the function $\kappa(r_*)$.

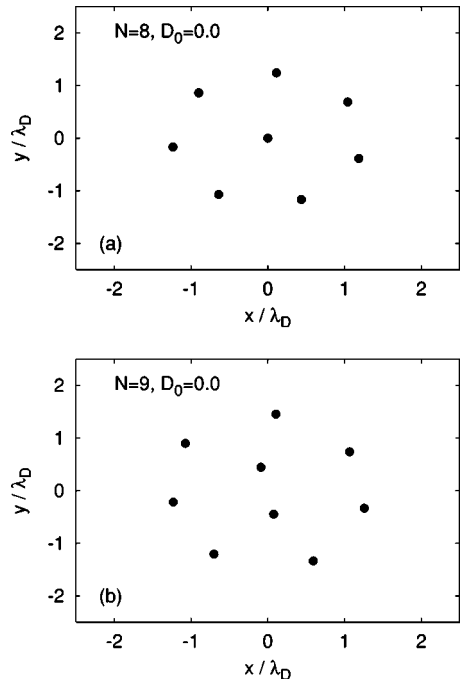

FIG. 3. Ground-state configurations of Coulomb crystals consisting of (a) $N=8$ and (b) $N=9$ grains, symbolized by the black dots. In each simulation we used an arbitrarily chosen friction parameter $\gamma_0=1$ (in c.u.) and $\kappa=1.03$, which is consistent with the data given in Table I. Each simulation run was stopped at $t=100$ (in c.u.) and the integration step was chosen as $\Delta t=0.0001$.

A. The case $N=2$

For the case $N=2$ it is possible to derive some simple analytical estimates for the ground-state configuration. To this end, consider the potential energy

$$U(\mathbf{r}_1,\mathbf{r}_2)=\frac{1}{2}(\mathbf{r}_1^2+\mathbf{r}_2^2)+\frac{\kappa}{r_{ij}}\exp(-r_{ij}). \tag{30}$$

By definition, each ground-state configuration $(\mathbf{r}_1^*,\mathbf{r}_2^*)=(x_1^*,y_1^*,x_2^*,y_2^*)$ must minimize U. For symmetry reasons, such a configuration must satisfy

$$x_1^*=-x_2^*, \quad y_1^*=-y_2^*. \tag{31}$$

If we introduce

$$r_*=(x_1^*)^2+(y_1^*)^2, \tag{32}$$

then r_* must be determined such that

$$U(\mathbf{r}_1^*,\mathbf{r}_2^*)=r_*^2+\frac{\kappa}{2r_*}\exp(-2r_*)\equiv U(r_*) \tag{33}$$

is a minimum. From the condition $U'(r_*)=0$ we thus get the transcendental equation

$$2r_*-\kappa\exp(-2r_*)\left(\frac{1}{r_*}+\frac{1}{2r_*^2}\right)=0. \tag{34}$$

In Fig. 2(a) the solution of this equation is plotted as the function $\kappa(r_*)$. The ground-state distance between the two grains for a given value κ is then given by $2r_*(\kappa)$. In Fig. 2(b) we also show a numerically found ground-state configuration (for details concerning the simulations, see Sec. IV B).

B. Ground-state configurations for $N>2$

In the previous section we briefly discussed the ground-state configuration for the case $N=2$. For more complex two-dimensional Coulomb clusters with $N\geqslant 3$, analytical studies become more complicated or even impossible. Nevertheless, one can identify the respective ground-state configurations by applying numerical methods. On the basis of Monte Carlo simulations such an analysis was performed by, e.g., Bedanov and Peeters [5]. In the present paper we pursue an alternative approach based on direct numerical simulations of the Langevin equations (29). More exactly, in order to identify the ground-state configurations we consider the deterministic limit, characterized by $D_0=0$ and $\gamma(v)\equiv\gamma_0>0$. Due to the pure damping, the system will eventually approach a state of minimal energy; i.e., all grains come to rest and constitute a stable configuration.

In Fig. 3 one can see the numerically obtained ground-state configurations for grain numbers $N=8$ and $N=9$. The shell structures agree with those found in the Monte Carlo simulations of Bedanov and Peeters [5]. In our simulations of the Langevin equations (29) we used a simple Euler scheme with an integration time step $\Delta t=0.0001$ (in c.u.) and randomly chosen initial conditions.

C. Normal modes

In the experiments of Melzer *et al.* [18] the normal modes of cluster oscillations were determined from a single more

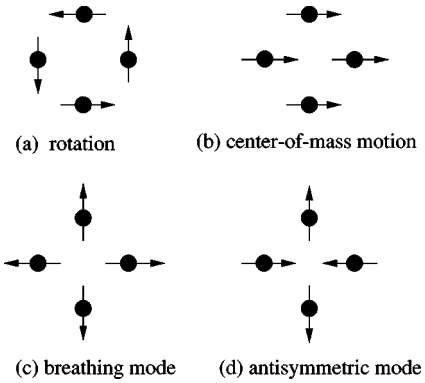

FIG. 4. The four different normal modes for a Coulomb cluster with $N=4$ particles.

complex oscillation, representing a superposition of the normal modes. As illustrated in Fig. 4, for $N=4$ grains there exist four normal modes, which can be identified as (a) rotation, (b) center-of-mass oscillation, (c) the breathing mode, and (d) the antisymmetric mode. Any more complex excitation of a Coulomb cluster can be represented as a superposition of the normal modes (or eigenmodes, respectively).

Figure 5 shows numerical results for the normal modes in a Coulomb cluster with $N=4$ grains, obtained from numerical integrations of the Langevin equations (29). The parameters in the simulations are chosen similar to those in the experiments of Melzer *et al.* [18] and listed in Table III. In the experiments of Melzer *et al.* [18] the modes were excited by a pulse modulation of the trap potential. As long as the pulse signal is present the cluster is quenched. After the signal is switched off, the cluster tends to relax to its original size and thus starts to oscillate. Since the grains are slowed down by collisions with neutrals in the plasma, these oscillations are damped. In our simulations each mode can be excited separately by choosing appropriate initial conditions.

As is particularly evident in Fig. 5(a), the simulated modes always exhibit (small) fluctuations around the perfectly unperturbed modes due to the presence of the heat bath (white noise). In general, our numerical results are in good agreement with the experimental results described in Ref. [18]. This fact supports the hypothesis that the Langevin approach provides a useful tool in order to theoretically investigate the dynamics of finite-size Coulomb crystals.

D. Angular momentum distributions

In the previous two subsections it was shown that the Langevin approach can successfully be used to find the ground-state configuration and describe the Brownian dynamics of Coulomb grains in a surrounding plasma. Furthermore, by numerically integrating the Langevin equations of motion (29a)–(29c) one can calculate the stationary probability distributions for arbitrary physical observables. With regard to our subsequent investigations of negative friction effects, it turns out to be useful to focus on the probability density function $f(L)$, where

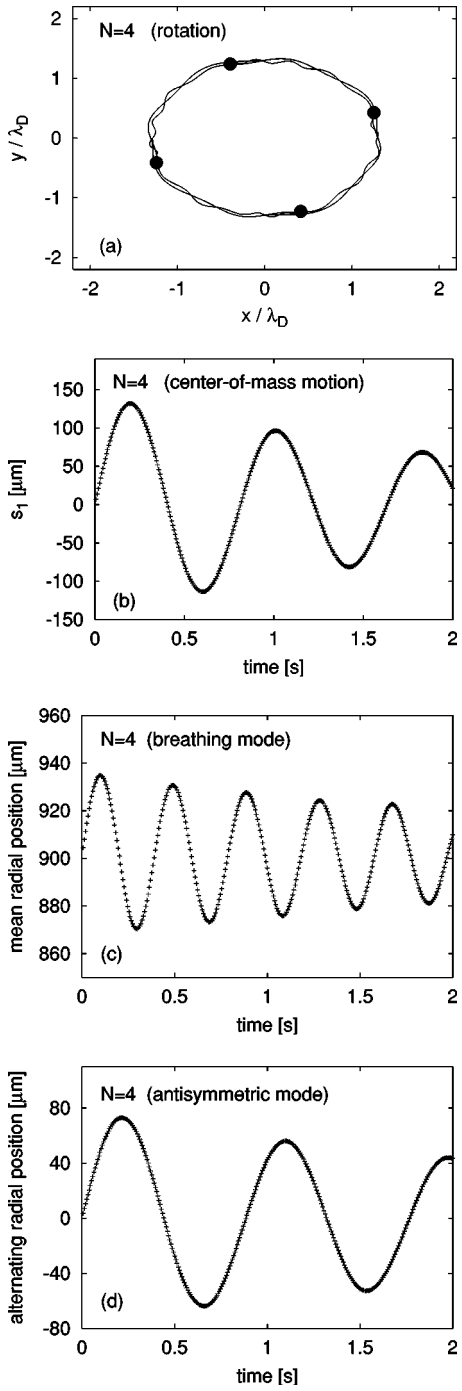

FIG. 5. Normal modes for $N=4$ particles and parameters as listed in Table III. Due to the positive friction coefficient $\gamma_0 = 0.7\ \mathrm{s}^{-1}$ the modes are damped out as $t\to\infty$. (a) Rotation around the center of the potential well: The diagram shows the orbits of the particles. The fluctuations from the circular orbit are caused by the stochastic force. (b) Center-of-mass oscillations: Here the oscillations of the x projection of the center-of-mass-coordinate $\boldsymbol{s} = (1/4)\Sigma_{i=1}^{4}\, \boldsymbol{r}_i$ are shown. (c) Breathing mode: The oscillations of the mean radial position $\langle r\rangle = (1/4)\Sigma_{i=1}^{4}\,(x_i^2+y_i^2)^{1/2}$ are plotted. (d) Antisymmetric mode: This diagrams shows the oscillations of the alternating sum $(1/4)\Sigma_{i=1}^{4}\,(-1)^{i+1}(x_i^2+y_i^2)^{1/2}$. (b)-(d) are arranged such that they can be directly compared with Figs. 2(b)–2(d) in Refs. [18].

TABLE III. Parameter values as used in the simulations of the normal modes, illustrated in Fig. 5. By virtue of the Einstein relation $T=m_g D_0/(\gamma_0 k)$, one finds that the parameters given below correspond to $T=285.64$ K.

Quantity	Symbol	Value (SI units)	Value (c.u.)
Grain radius	a	4.74 μm	0.0068
Grain mass	m_g	6.73×10^{-13} kg	1
Grain charge	Q	$-18000e$	-18000
Debye length	λ_D	700 μm	1
Viscous friction coefficient	γ_0	0.7 s^{-1}	0.091
Noise amplitude	D_0	4.1×10^{-9} m^2 s^{-3}	1.8×10^{-5}
Trap frequency	ω_0	7.7 s^{-1}	1

$$L=\frac{1}{N}\sum_{i=1}^{N}L_i=\frac{1}{N}\sum_{i=1}^{N}m_g(x_i v_{yi}-y_i v_{xi}) \tag{35}$$

is the overall angular momentum normalized to one particle. Figure 6 shows the numerically calculated function $f(L)$ for the case of $N=2$ grains and parameters $\gamma_0=1.0$, $D_0=0.001$ (we continue to use c.u. defined by $m_g=\omega_0=\lambda_D=e=1$). The probability density $f(L)$ was determined from a histogram, numerically calculated over the time interval $[0;10000]$ (in c.u.). As one can see in Fig. 6, the function $f(L)$ possesses an approximately Gaussian shape, centered around $L=0$. Qualitatively very similar results are found for $N=1$ and $N=3$ (not shown here); that is, in these cases also the distributions exhibit a single maximum at $L=0$ and decay monotonically for $|L|>0$. This behavior can be readily understood if one considers the equilibrium stochastic dynamics of the grains. In the presence of constant positive friction $\gamma(v)=\gamma_0$ and sufficiently low temperature T, corresponding to small values D_0, the particles weakly oscillate around the ground state, which is characterized by $L=0$.

As we shall see later, the angular momentum probability density $f(L)$ will look essentially different in the presence of negative friction.

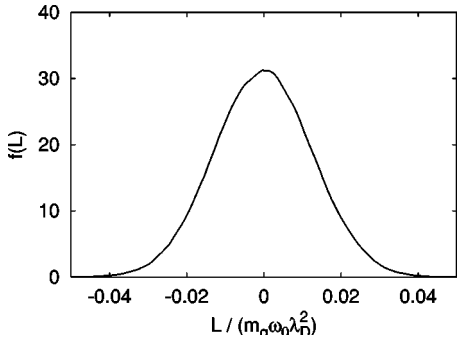

FIG. 6. Angular momentum probability density function $f(L)$ for $N=2$ grains, numerically calculated over the time interval $[0;10000]$ (in c.u.). Further parameters used in this simulation are $\kappa=1.03$, $\gamma_0=1.0$, $D_0=0.001$, and integration time step $\Delta t=0.0001$ (in c.u.). The shape of the density function $f(L)$ is very similar for $N=2,3$ (not shown here).

V. NEGATIVE (ACTIVE) FRICTION

In the previous Sec. IV we concentrated on constant positive friction coefficients $\gamma(v)\equiv\gamma_0>0$. In the remainder we focus on the effects of negative friction. More exactly, it is assumed that the effective friction coefficient is given by the Rayleigh approximation [34] from Eq. (5); that is, we exclusively consider $\gamma(v)=\alpha(v^2-v_0^2)$ from now on. Additionally, we shall make the simplifying assumption that the noise amplitude is approximately constant, $D(v)\approx D_0$. In all simulations the parameters α, v_0, and D_0 are treated as independent parameters. As will become clear below, the influence of negative friction leads to complex stationary motions of a Coulomb cluster, which can be identified as rotations or oscillating modes.

In order to get an idea of the effects of negative friction, it is helpful to consider the deterministic limit case, corresponding to $D_0=0$, first. This will be done in Sec. V A. The more general case $D_0>0$ is discussed subsequently in Sec. V B. As before we use characteristic units (c.u.) defined by $m_g=\omega_0=\lambda_D=e=1$ throughout this section.

A. Deterministic dynamics ($D_0=0$)

In the limiting case $D_0=0$ the originally stochastic equations of motions (29) reduce to a set of ordinary deterministic differential equations. Hence, depending on the initial conditions, the dissipative system will approach a stable stationary state, corresponding to a special sub-manifold (attractor) in the phase space. For grain numbers $N=1,2$ one can find analytical estimates for the attractors, while for $N>2$ analytical studies become extremely difficult. Nevertheless, the general structure of the attractors can already be well understood on the basis of the results obtained for the two simplest cases $N=1,2$.

1. The case $N=1$

Here the grain-grain Coulomb interaction is irrelevant. Hence, for $D_0=0$ the dynamical equations (29b) reduce to

$$\dot{\boldsymbol{v}}=-\boldsymbol{r}-\alpha(\boldsymbol{v}^2-v_0^2)\boldsymbol{v}. \tag{36}$$

The related stable stationary motions (limit cycles) correspond to cyclic rotations with constant radius r_0 around the center of the trap. Obviously, they must satisfy the condition

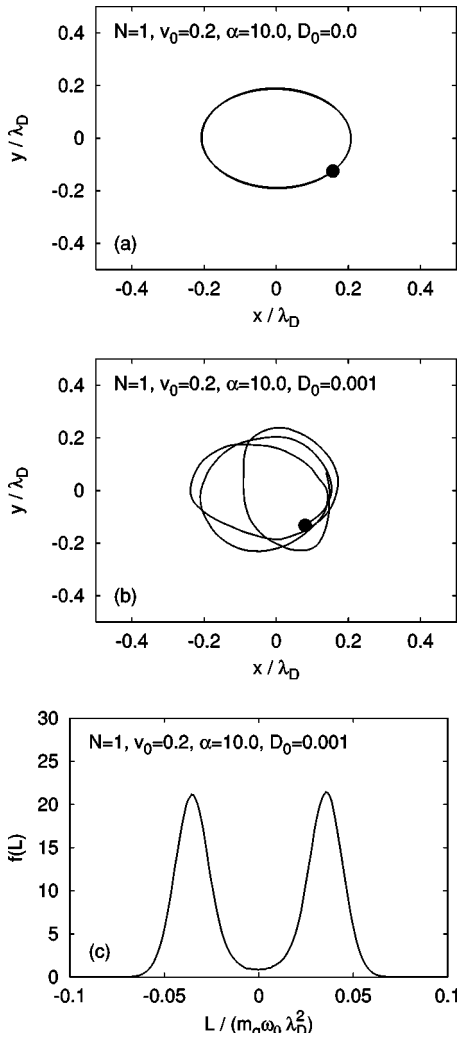

FIG. 7. Dynamics of a single grain, $N=1$, moving in the trap under the influence of active friction. (a) Limit cycle in the (x,y) plane for deterministic grain motion in the limit case $D_0=0$. (b) For $D_0>0$ the grain performs a stochastic motion in the trap, which is plotted here for the time interval [99 980; 100 000] (in c.u.). Due to the influence of the stochastic force, the motion of the grain deviates from the exact attractor. As shown in (c), this results in the double-peaked shape of the angular momentum probability density $f(L)$. The function $f(L)$ is calculated from a histogram, reflecting the L distribution over the time interval [0; 100 000] (in c.u.). As in the previous simulations the integration time step $\Delta t=0.0001$ (in c.u.) was used.

$$\boldsymbol{v}^2 = v_0^2 = r_0^2. \tag{37}$$

Figure 7 shows the projection of these limit cycles on the horizontal (x,y) plane of the trap.

2. The case $N=2$

For $D_0=0$ and $N=2$ the dynamical equations (29b) read

$$\dot{\boldsymbol{v}}_1 = -\boldsymbol{r}_1 + \boldsymbol{F}_1^{\mathrm{C}} - \alpha(\boldsymbol{v}_1^2 - v_0^2)\,\boldsymbol{v}_1, \tag{38a}$$

$$\dot{\boldsymbol{v}}_2 = -\boldsymbol{r}_2 + \boldsymbol{F}_2^{\mathrm{C}} - \alpha(\boldsymbol{v}_2^2 - v_0^2)\boldsymbol{v}_2, \tag{38b}$$

where

$$\boldsymbol{F}_1^{\mathrm{C}} = \kappa\frac{\boldsymbol{r}_1-\boldsymbol{r}_2}{|\boldsymbol{r}_1-\boldsymbol{r}_2|^3}\exp(-|\boldsymbol{r}_1-\boldsymbol{r}_2|)(1+|\boldsymbol{r}_1-\boldsymbol{r}_2|) = -\boldsymbol{F}_2^{\mathrm{C}}. \tag{38c}$$

The first attractor of the dynamical system (38) corresponds to an equidistant rotation of the grains around the center of the trap [see Fig. 8(b)]. The stationary motions of the grains on this attractor are uniquely determined by the following conditions:

$$\boldsymbol{r}_1 = -\boldsymbol{r}_2, \quad \boldsymbol{r}_1^2 = \boldsymbol{r}_2^2 = r_0^2, \tag{39a}$$

$$\boldsymbol{v}_1 = -\boldsymbol{v}_2, \quad \boldsymbol{v}_1^2 = \boldsymbol{v}_2^2 = v_0^2, \tag{39b}$$

where r_0 and v_0 are connected as follows:

$$\frac{v_0^2}{r_0} = r_0 - \kappa\frac{\exp(-2r_0)}{4r_0^2}(1+2r_0). \tag{39c}$$

Obviously, the condition (39b) makes sure that the two friction force terms in Eq. (38) vanish. Moreover, according to Eq. (39a), the grains rotate diametrically around the center of the trap with constant distance $2r_0$ between each other. Depending on the initial conditions, the rotations of the grains occur either clockwise or counterclockwise. The last condition (39c) reflects the compensation of radial and centripetal forces on the attractor. In Fig. 8(a) one can see a plot of the related function $v_0(r_0)$. In particular, we note that the condition (39c) reduces to the earlier result (34) in the limit case $v_0=0$.

The *rotation attractors* just described are not the only stable stationary motions in the case of $N=2$. In order to identify a second type of attractor, we introduce the center-of-mass coordinates $\boldsymbol{s}$ and relative coordinates $\boldsymbol{r}$ by

$$\boldsymbol{s} = \frac{1}{2}(\boldsymbol{r}_1+\boldsymbol{r}_2), \quad \boldsymbol{r} = \boldsymbol{r}_2 - \boldsymbol{r}_1. \tag{40}$$

The related velocities $\boldsymbol{u}=\dot{\boldsymbol{s}}$ and $\boldsymbol{w}=\dot{\boldsymbol{r}}$ read

$$\boldsymbol{u} = \frac{1}{2}(\boldsymbol{v}_1+\boldsymbol{v}_2), \quad \boldsymbol{w} = \boldsymbol{v}_2 - \boldsymbol{v}_1. \tag{41}$$

Using Eq. (38) one thus finds

$$\dot{\boldsymbol{u}} = -\boldsymbol{s} - \alpha\left[2\left(\boldsymbol{u}^2 + \frac{1}{4}\boldsymbol{w}^2 - v_0^2\right)\boldsymbol{u} + (\boldsymbol{u}\boldsymbol{w})\boldsymbol{w}\right], \tag{42a}$$

$$\dot{\boldsymbol{w}} = -\boldsymbol{r} + 2\kappa\frac{\boldsymbol{r}}{|\boldsymbol{r}|^3}\exp(-|\boldsymbol{r}|)(1+|\boldsymbol{r}|) - \alpha\left[2(\boldsymbol{u}\boldsymbol{w})\boldsymbol{u} + \left(\boldsymbol{u}^2 + \frac{1}{4}\boldsymbol{w}^2 - v_0^2\right)\boldsymbol{w}\right]. \tag{42b}$$

Obviously, a stationary solution of these two equations is given by

$$\boldsymbol{w} = \boldsymbol{0}, \quad |\boldsymbol{r}| = r^*, \tag{43a}$$

$$\boldsymbol{u}^2 = v_0^2, \quad |\boldsymbol{s}| = s^*, \tag{43b}$$

provided the constants r^* and s^* are solutions of the following two equations:

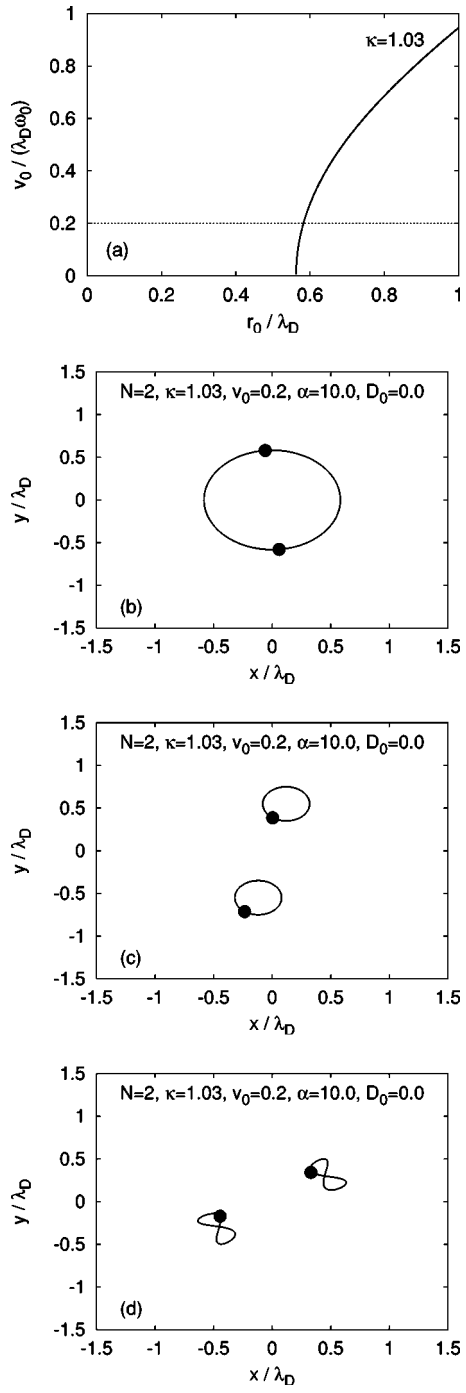

FIG. 8. Attractors for the active motions of $N=2$ grains in the deterministic limit $D_0=0$. (a) Function $v_0(r_0)$ from Eq. (39c) plotted for the same parameter κ as used in the numerical simulations of the orbits shown in diagrams (b)–(d). (b) Rotation attractor: The intersection point of the thin horizontal line $v_0=0.2$ with the curve $v_0(r_0)$ in (a) determines the stationary distance $d=2r_0$ of the grains, if this attractor is approached. (c) Acoustical oscillation attractor: The orbits of this attractor type correspond to a stationary center-of-mass rotation with constant relative vector $\boldsymbol{r}=\boldsymbol{r}_2-\boldsymbol{r}_1$ between the grains. (d) Optical oscillation attractor: Here the orbits of the grains result from a superposition of center-of-mass oscillations and radial oscillations.

TABLE IV. Absolute time average values $|\langle L\rangle|$ for the three different attractor types found for $N=2$. The parameters are the same as those used in Figs. 8(b)–8(d).

Attractor type	$\lvert\langle L\rangle\rvert$ (c.u.)
Rotation	0.12
Acoustical oscillation	0.04
Optical oscillation	0

$$0 = r^* - 2\kappa \frac{\exp(-r^*)}{r^{*2}}(1+r^*), \tag{43c}$$

$$\frac{v_0^2}{s^*} = s^*. \tag{43d}$$

The condition (43c) exactly corresponds to the earlier result (34) and (43d) reflects the compensation of the centrifugal force and the harmonic (trap) force with respect to the center-of-mass coordinate $\boldsymbol{s}$. Figure 8(c) shows an example for the orbits determined by Eqs. (43). As one can see in this picture, the difference vector $\boldsymbol{r}=\boldsymbol{r}_2-\boldsymbol{r}_1$ remains fixed, as indicated by Eq. (43a), whereas the center-of-mass coordinate performs a stationary rotation with radius $s^*=v_0$ around the center of the trap. Since the relative coordinate remains fixed, we shall refer to this attractor type as an *acoustical oscillation.*

In addition to the rotation attractor from Fig. 8(b) and the acoustical attractor from Fig. 8(c), one can still find a third type of stable motion, which is represented in Fig. 8(d). The orbits related to this attractor are more complex and can be explained as a superposition of radial oscillations and center-of-mass oscillations. In the following, the attractor in Fig. 8(d) will be referred to as a stationary *optical oscillation.*

In order to find out whether there still exist further types of stable stationary motions for $N=2$ grains, we have calculated the orbits for a large number of randomly chosen initial conditions. In these simulations the grains always approached one of the above attractors. Therefore, it seems plausible to assume that the set of attractors in Figs. 8(b)–8(d) is complete. This assumption is supported by the close relationship between the above three attractor types and the three normal modes of the Coulomb cluster with two grains: rotation, center-of-mass motion, and optical oscillations (breathing mode).

With regard to the subsequent discussion of the stochastic dynamics ($D_0>0$) it is important to note that each of the attractor types is characterized by a characteristic time average value

$$\langle L\rangle = \lim_{t\to 0}\frac{1}{\tau}\int_0^\tau dt\, L, \tag{44}$$

where the mean overall angular momentum L was defined in Eq. (35). In Table IV, we have listed the respective numerical values $|\langle L\rangle|$, based on the same simulation parameters as used in Figs. 8(b)–8(d). Below, the knowledge of these val-

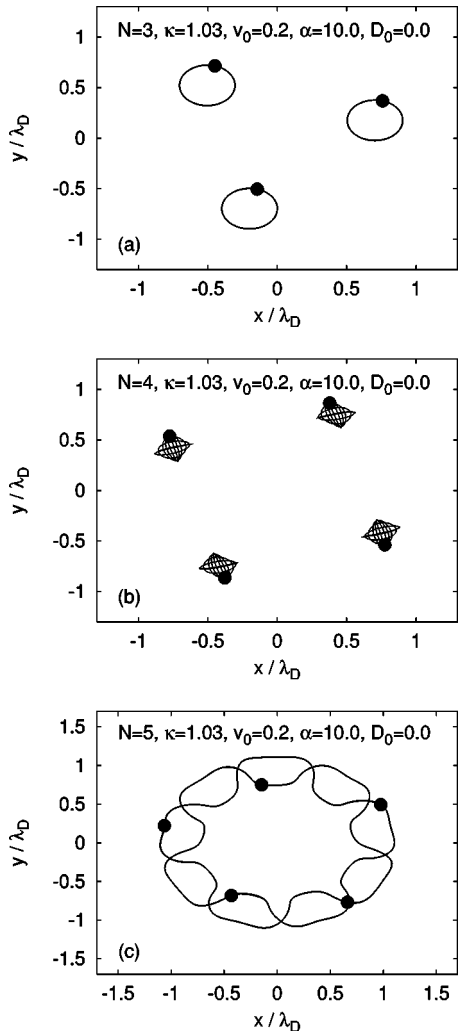

FIG. 9. Examples of stationary active motions for Coulomb clusters with $N=3,4,5$ grains. (a) $N=3$: A comparison with Fig. 8(c) reveals that this attractor corresponds to the acoustical oscillation. (b) $N=4$: For this stable optical excitation [compare Fig. 8(d)], the stationary orbit of a single grain is very similar to a Lissajous-pattern. (c) $N=5$: This attractor form is different in the case $N=2$ from Fig. 8.

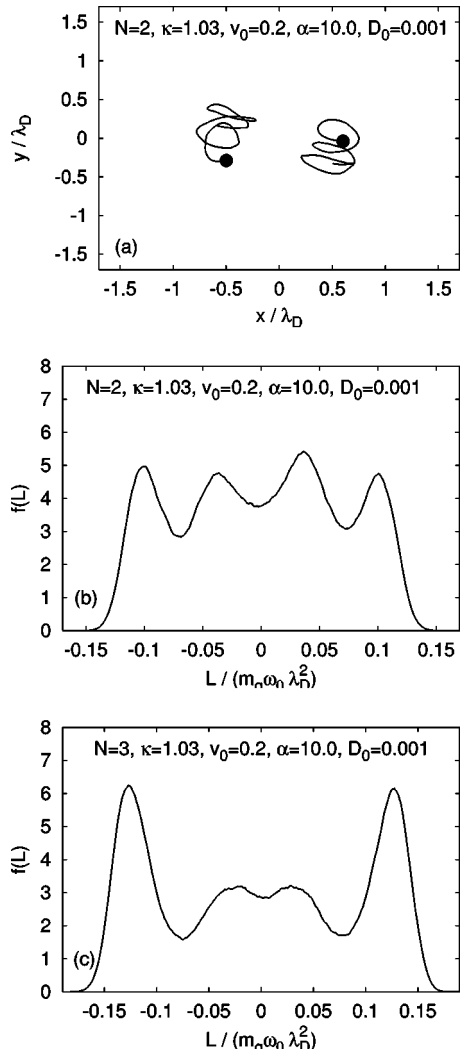

FIG. 10. (a) For $D_0>0$ the two grains performs a stochastic motion around the center of the trap, plotted here for the time interval [99 980; 100 000] (in c.u.). Due to the influence of the stochastic force, the system can travel between the different attractor regions of the related deterministic system. (b) Angular momentum probability density $f(L)$ for the case $N=2$, numerically calculated over the time interval [0; 100 000] (in c.u.). The peaks of the distribution are located at the L values that characterize the attractors of the corresponding deterministic system with $D_0=0$. (c) Angular momentum probability density $f(L)$ for the case $N=3$, numerically calculated over the time interval [0; 100 000] (in c.u.). In all simulations the integration time step is chosen as $\Delta t=0.0001$ (in c.u.).

ues will help us to understand the shape of the angular momentum distribution $f(L)$.

3. Attractors for $N>2$

In Fig. 9 one can see some examples of numerically calculated stable orbits for active Coulomb clusters with $N=3,4,5$ grains. While some of these attractors exhibit a structure that is very similar to those observed for $N=2$, there also appear new types of stationary motions [see Fig. 9(c)]. In principle, the number of attractors steadily increases with particle number N. This observation is explained by the fact that the number of normal modes also increases with N. More generally speaking, each of the observed attractors seems to be closely related to one of the normal modes of the related conservative system. This observation supports the following more general hypothesis [55]: If the friction coefficient is similar to Rayleigh's model, then each attractor of the system must be very similar to one of the eigenmodes of the corresponding conservative system; in particular, there seems to exist a fixed relationship between the number of attractors and the number of eigenmodes (or normal modes, respectively).

B. Stochastic dynamics ($D_0>0$)

While the previous subsection was dedicated to the dynamical attractors in the deterministic limit case $D_0=0$, we shall now also consider the effects of a stochastic force com-

ponent. For $D_0 > 0$ the stationary dynamics of our model system is not confined to a single attractor basin anymore. If, however, the parameters α and κ are sufficiently large, then the stochastic system with D_0 is also spending a relatively long time in the vicinity of the attractor regions of the related deterministic system with $D_0 = 0$. This is illustrated in Figs. 7(b) and 10(a), where we plotted the stochastic orbits for $N = 1$ and $N = 2$, respectively.

The transitions between the different attractor regions are also reflected by the angular momentum probability density $f(L)$. For active friction the shape of this function essentially differs from the approximately Gaussian distribution, which was found earlier in the case of passive friction (Fig. 6). As shown in Fig. 7(c), for $N = 1$ the density $f(L)$ exhibits two maxima located near $|L| = 0.04$, which is just the angular momentum value for a grain moving on the attractor in Fig. 7(a).

Similarly, for $N = 2$ the function $f(L)$ exhibits four peaks [see Fig. 10(b)]. By virtue of Table IV, these peaks can be identified with the rotation attractor and the acoustical oscillation attractor from Figs. 8(b) and 8(c). Merely the central peak at $L = 0$, corresponding to the optical mode, is suppressed. A plausible explanation for this fact is that this attractor is not very stable with respect to fluctuations.

VI. SUMMARY

During the past decade, Coulomb clusters confined by an external harmonic trap potential have attracted considerable experimental and theoretical interest [1–5,7,18]. In the present paper, the Brownian dynamics of finite-size Coulomb clusters was studied numerically and analytically on the basis of a Langevin approach. In particular, the influence of passive and active friction was investigated.

Passive friction is characterized by a positive friction coefficient and arises primarily due to grain–neutral-atom interactions in dusty plasmas. Here, we considered this (rather usual) case in order to show that the Langevin approach can successfully describe the Brownian dynamics of charged grains in a plasma. More exactly, it was shown that numerical integration of the Langevin equations of motion yields the correct ground-state configurations (Sec. IV B) as well as the correct normal modes (Sec. IV C), known from recent experiments [18] and theoretical work [1].

As outlined in Secs. I and II, in some dusty plasma models there also appears active friction [41,46,50]. Active friction means that the effective friction coefficient becomes negative at small grain velocities. Thus, active friction may result in complex stable excitations of a Coulomb crystal. In particular, in such models the mean kinetic energy associated with active grain motions can be much larger than the mean thermal energy. Fortov *et al.* [9] report that in several of their experiments the "apparent temperature" of the grains is in the range $(2 \times 10^5 - 5 \times 10^5)$ K, which is approximately 10^3 times higher than the temperature of the ions in the surrounding plasma. We suggest that the development of the concept of active friction might be helpful in order to explain such observations.

As indicated by the numerical results in Secs. IV D and V B, measurements of velocity distributions and angular momentum distributions may help to answer the question of whether active friction is actually present or not. In the case of purely passive friction the angular momentum distribution is characterized by an approximately Gaussian shape, whereas it exhibits several different maxima in systems with active friction.

In summary, direct simulation of the Langevin equations provides a useful tool in order to investigate the spatiotemporal dynamics of finite Coulomb clusters. In principle, this method can easily be applied to test microscopic models underlying friction and velocity diffusion coefficients. A general approach to the calculation of these coefficients is, e.g., discussed in Ref. [50]. Nevertheless a satisfactory theory, which models the very complex energy transfer processes between nonequilibrium plasmas and grains, is still missing. Possible future applications of the Langevin method could also include time-resolved numerical studies of heating and melting phenomena in clusters.

With regard to experiments, however, the most interesting question is whether it is possible to realize plasma conditions such that active motions of grains in a plane can be studied in detail. In particular, it would be very interesting to learn whether experimentally measured velocity distributions do indeed show deviations from a Maxwellian distribution as discussed in the present work.

ACKNOWLEDGMENTS

The authors are very grateful to M. Bonitz, V. E. Fortov, G. J. F. van Heijst, G. M. W. Kroesen, A. Melzer, O. F. Petrov, G. Roepke, L. Schimansky-Geier, P. P. J. M. Schram, and W. W. Stoffels for numerous helpful discussions.

[1] M. Kong, B. Partoens, and F. M. Peeters, New J. Phys. **5**, 23 (2003).
[2] Y. E. Lozovik and L. M. Pomirchy, Phys. Status Solidi B **161**, K11 (1990).
[3] Y. E. Lozovik and V. A. Mandelshtam, Phys. Lett. A **145**, 269 (1990).
[4] F. Bolton and U. Rössler, Superlattices Microstruct. **13**, 193 (1993).
[5] V. M. Bedanov and F. M. Peeters, Phys. Rev. B **49**, 2667 (1994).
[6] J. H. Chu and Lin I, Phys. Rev. Lett. **72**, 4009 (1994).
[7] M. Klindworth, A. Melzer, A. Piel, and V. A. Schweigert, Phys. Rev. B **61**, 8404 (2000).
[8] A. P. Nefedov *et al.*, J. Exp. Theor. Phys. **95**, 673 (2002).
[9] V. E. Fortov *et al.*, J. Exp. Theor. Phys. **96**, 704 (2003).
[10] V. A. Schweigert and F. M. Peeters, Phys. Rev. B **51**, 7700 (1995).
[11] M. Bonitz, V. Golubnychiy, A. Filinov, and Y. E. Lozovik,

Microelectron. Eng. **62**, 141 (2002).
[12] A. Melzer, T. Trottenberg, and A. Piel, Phys. Lett. A **191**, 301 (1994).
[13] H. Thomas, G. E. Morfill, V. Demmel, J. Goree, B. Feuerbacher, and D. Möhlmann, Phys. Rev. Lett. **73**, 652 (1994).
[14] H. M. Thomas and G. E. Morfill, Nature (London) **379**, 806 (1996).
[15] J. Goree, Phys. Rev. Lett. **69**, 277 (1992).
[16] V. E. Fortov, A. N. Nefedov, and O. F. Petrov, Phys. Usp. **40**, 1163 (1997).
[17] W.-T. Juan, Z.-H. Huang, J.-W. Hsu, Y.-J. Lai, and Lin I, Phys. Rev. E **58**, R6947 (1998).
[18] A. Melzer, M. Klindworth, and A. Piel, Phys. Rev. Lett. **87**, 115002 (2001).
[19] R. P. Dahiya, G. V. Paeva, W. W. Stoffels, E. Stoffels, G. M. W. Kroesen, K. Avinash, and A. Bhattacharjee, Phys. Rev. Lett. **89**, 125001 (2002).
[20] P. K. Shukla and A. A. Mamun, *Introduction to Dusty Plasmas Physics* (IOP, Bristol, 2001).
[21] D. P. Resindes, R. Bingham, and V. N. Tsytovich, J. Plasma Phys. **49**, 458 (1996).
[22] P. K. Shukla, M. Y. Yu, and R. Bharuthram, J. Geophys. Res., [Atmos.] **93**, 346 (1991).
[23] N. N. Rao, P. K. Shukla, and M. Y. Yu, Planet. Space Sci. **38**, 543 (1990).
[24] S. A. Trigger and P. P. J. M. Schram, J. Phys. D **32**, 234 (1999).
[25] A. Barkan, R. L. Merlino, and N. D'Angelo, Phys. Plasmas **2**, 3563 (1995).
[26] C. Thomson, A. Barkan, N. D'Angelo, and R. L. Merlino, Phys. Plasmas **4**, 2331 (1997).
[27] W. Ebeling and G. Röpke, Physica D **187**, 268 (2004).
[28] A. Melzer, A. Homann, and A. Piel, Phys. Rev. E **53**, 2757 (1996).
[29] V. N. Tsytovich, G. E. Morfill, and H. Thomas, Plasma Phys. Rep. **28**, 623 (2002).
[30] G. E. Morfill, V. N. Tsytovich, and H. Thomas, Plasma Phys. Rep. **29**, 1 (2003).
[31] V. N. Tsytovich, Usp. Fiz. Nauk **40**, 53 (1997).
[32] F. Verheest, *Waves in Dusty Space Plasmas* (Kluwer, Dordrecht, 2000).
[33] P. Bliokh, V. Sinitsin, and V. Yaroshenko, *Dusty and Self-Gravitational Plasmas in Space* (Kluwer, Dordrecht, 1995).
[34] J. W. Rayleigh, *The Theory of Sound*, 2nd ed. (Dover, New York, 1945), Vol. 1.
[35] A. G. Zagorodny, P. P. J. M. Schram, and S. A. Trigger, Phys. Rev. Lett. **84**, 3594 (2000).
[36] P. P. J. M. Schram, A. G. Sitenko, S. A. Trigger, and A. G. Zagorodny, Phys. Rev. E **63**, 016403 (2000).
[37] S. A. Trigger, Contrib. Plasma Phys. **41**, 331 (2001).
[38] A. M. Ignatov, S. A. Trigger, W. Ebeling, and P. P. J. M. Schram, Phys. Lett. A **293**, 141 (2001).
[39] S. A. Khrapak, A. V. Ivlev, G. E. Morfill, and H. M. Thomas, Phys. Rev. E **66**, 046414 (2002).
[40] P. P. J. M. Schram, S. A. Trigger, and A. G. Zagarodny, New J. Phys. **5**, 27 (2003).
[41] S. A. Trigger and A. Zagorodny, Contrib. Plasma Phys. **43**, 381 (2003).
[42] M. Schienbein, K. Franke, and H. Gruler, Phys. Rev. E **49**, 5462 (1994).
[43] F. Schweitzer, W. Ebeling, and B. Tilch, Phys. Rev. Lett. **80**, 5044 (1998).
[44] U. Erdmann, W. Ebeling, L. Schimansky-Geier, and F. Schweitzer, Eur. Phys. J. B **15**, 105 (2000).
[45] F. Schweitzer, W. Ebeling, and B. Tilch, Phys. Rev. E **64**, 021110 (2001).
[46] S. A. Trigger, W. Ebeling, A. M. Ignatov, and I. Tkachenko, Contrib. Plasma Phys. **43**, 377 (2003).
[47] W. Ebeling, F. Schweitzer, and B. Tilch, BioSystems **49**, 17 (1999).
[48] U. Erdmann, W. Ebeling, and V. S. Anishchenko, Phys. Rev. E **65**, 061106 (2002).
[49] P. S. Epstein, Phys. Rev. **23**, 710 (1924).
[50] S. A. Trigger, Phys. Rev. E **67**, 046403 (2003).
[51] S. A. Khrapak, A. V. Ivlev, G. E. Morfill, and S. K. Zhdanov, Phys. Rev. Lett. **90**, 225002 (2003).
[52] G. A. Hebner, M. E. Riley, D. S. Johnson, P. Ho, and R. J. Buss, Phys. Rev. Lett. **87**, 235001 (2001).
[53] Y.-J. Lai and Lin I, Phys. Rev. E **60**, 4743 (1999).
[54] T. Matsoukas and M. Russell, Phys. Rev. E **55**, 991 (1997).
[55] J. Dunkel, W. Ebeling, U. Erdmann, and V. A. Makarov, Int. J. Bifurcation Chaos Appl. Sci. Eng. **12**, 2359 (2002).